

A Coordination Architecture for Spacecraft Formation Control

Randal W. Beard, *Member, IEEE*, Jonathan Lawton, *Member, IEEE*, and Fred Y. Hadaegh, *Senior Member, IEEE*

Abstract—This paper addresses the problem of coordinating multiple spacecraft to fly in tightly controlled formations. The main contribution of the paper is to introduce a coordination architecture that subsumes leader-following, behavioral, and virtual-structure approaches to the multiagent coordination problem. The architecture is illustrated through a detailed application of the ideas to the problem of synthesizing a multiple spacecraft interferometer in deep space.

Index Terms—Control architecture, coordinated control, interferometry, spacecraft formation flying.

I. INTRODUCTION

THE CONCEPT of multiple spacecraft flying in formation is emerging as an attractive alternative to traditional monolithic spacecraft for both scientific and military applications. The multiple spacecraft approach has several advantages including, increased instrument resolution, reduced cost, reconfigurability, and overall system robustness. Some of the potential applications for formation flying include space-based interferometers and military surveillance instruments. Both NASA and the Air Force have identified spacecraft formation flying as a key technology for the 21st century.

In addition to research on spacecraft formation flying, there have also been a number of studies on coordinating the behavior of multiple robots and aircraft. While the application is different, the fundamental approaches to the coordination of multiple spacecraft, robots, and aircraft are very similar: the common theme being the coordination of multiple agents to accomplish an objective. There are roughly three approaches to multiagent coordination reported in the literature, namely leader-following, behavioral, and virtual structures.

In leader-following, one of the spacecraft is designated as the leader, with the rest of the spacecraft designated as followers. The basic idea is that the followers track the position and

orientation of the leader with some prescribed (possibly time varying) offset. There are numerous variations on this theme including designating multiple leaders, forming a chain (spacecraft i tracks spacecraft $i - 1$), and other tree topologies.

One of the first studies on leader-following strategies is reported in [1] which discusses formation control laws for mobile robots. The application of these ideas to spacecraft formations is reported in [2], where explicit control laws for formation keeping and relative attitude alignment based on nearest neighbor tracking are derived. Several leader-following techniques are discussed including leader tracking, nearest neighbor tracking, barycenter tracking, and other tree topologies. In [3], the ideas of [2] are extended to account for actuator saturation and are applied to the problem of controlling the formation to execute a continuous rotational slew. In [4], adaptive control laws are added to the control derived in [2] in order to reject common space disturbances. Leader-following approaches to satellite formation keeping in earth orbit are described in [5]–[7].

There have been a number of studies of leader-following techniques in the mobile robotics community. In [8], leader-following is used to control a group of mobile robots to cooperatively move a box. In [9], feedback linearization techniques are used to derive tracking control laws for nonholonomic robots that are used for leader-following. In addition, the authors describe the formation configuration as a directed graph. The shape of the formation is changed as graph structures are changed. Another approach to leader-following for multiple nonholonomic robots is described in [10]. A leader-following approach to the platoon problem in intelligent highways is contained in [11].

The basic idea behind the behavioral approach is to prescribe several desired behaviors for each agent, and to make the control action of each agent a weighted average of the control for each behavior. Possible behaviors include collision avoidance, obstacle avoidance, goal seeking, and formation keeping. There are also numerous variations on the behavioral approach to multiagent coordination, most of which are derived by novel weightings of the behaviors.

In [12], the behavioral approach is applied to the problem of maintaining a constellation of satellites in an equally distributed ring formation in earth orbit. Simple Lyapunov control functions are used to maintain distance and avoid collisions. The application of the behavioral approach to aircraft flying in formation is described in [13], where the control strategies are derived to mimic the instinctive behavior of birds and fish. A paper that describes the behavioral approach to formation keeping for mo-

Manuscript received July 7, 1999; revised August 2, 2000. Manuscript received in final form June 15, 2001. Recommended by Associate Editor D. W. Repperger. This work was performed in part at the Jet Propulsion Laboratory, California Institute of Technology, under contract with the National Aeronautics and Space Administration. The research at Brigham Young University (BYU) was supported by the Jet Propulsion Laboratory, California Institute of Technology, under Contract 96-1245.

R. W. Beard is with the Electrical and Computer Engineering Department, Brigham Young University (BYU), Provo, UT 84602 USA (e-mail: beard@ee.byu.edu).

J. Lawton is with the Raytheon Systems Company, Tucson, AZ 85734-1337 USA (e-mail: jonathan_r_lawton@west.raytheon.com).

F. Y. Hadaegh is with the Guidance and Control Section, Jet Propulsion Laboratory, California Institute of Technology, Pasadena, CA 91109-8099 USA (e-mail: Fred.Y.Hadaegh@jpl.nasa.gov).

Publisher Item Identifier S 1063-6536(01)09476-3.

mobile robots is [14] where control strategies are derived by averaging several competing behaviors including goal seeking, collision avoidance, and formation maintenance. Since competing behaviors are averaged, occasionally strange and unpredicted behaviors may occur. Unit-center tracking, leader tracking and nearest neighbor tracking controls are also studied. In [15], the behavioral approach is used to cause a group of robots to create line and circle formations. These ideas are extended in [16] to the problem of controlling a formation of mobile robots to transport objects.

In the virtual structure approach, the entire formation is treated as a single structure. For example, in an interferometry mission it may be desirable to have a constellation of spacecraft act as a single rigid body. In the virtual structure approach, the control is derived in three steps: first, the desired dynamics of the virtual structure are defined, second, the motion of the virtual structure is translated into the desired motion for each agent, and finally, tracking controls for each spacecraft are derived.

The virtual structure approach was applied to formations of mobile robots in [17]. The application to formations of spacecraft in free space is described in [18] and [19]. In Section III we will give a detailed example of the virtual structure approach to spacecraft formation control.

Besides the three approaches described above, there have been other studies of multiple satellites orbiting the earth in formation. Two spacecraft flying in a polar orbit formation is considered in [20] and [21], and a software package that implements their approach is described in [22]. In [23], the design of a two satellite formation flying mission for an interferometric SAR topography mission is described. Formation keeping for low-earth orbit satellites is considered in [24]. Relative formation keeping for low-earth orbits using linear quadratic (LQ) regulators is discussed in [25]. There have been several studies on optimal fuel formation control including [26]–[28].

Leader-following, behavioral, and virtual structure approaches to the coordination problem have their corresponding strengths and weakness. The strength of leader-following is that group behavior is directed by specifying the behavior of a single quantity: the leader. The weakness, however, is that there is no explicit feedback to the formation. For example, the leader may be moving too fast for the following agents to track. Another weakness is that the leader is a single point of failure for the formation. The strength of the behavioral approach is that it is natural to derive control strategies when agents have multiple competing objectives. In addition, there is explicit feedback to the formation since each agent reacts according to the position of its neighbors. Another strength is that the behavioral approach lends itself naturally to a decentralized implementation. The primary weakness is that group behavior cannot be explicitly defined, rather the group behavior is said to “emerge.” Another weakness is that behavioral approaches are difficult to analyze mathematically and characteristics of the formation (like stability) cannot generally be guaranteed. The strength of the virtual structure approach is that it is fairly easy to prescribe a coordinated behavior for the group. In addition, feedback to the virtual structure is naturally defined.

The disadvantage is that requiring the formation to act as a virtual structure limits the class of potential applications of this approach.

The objective of the current paper is to introduce an architecture that unifies the three approaches discussed above. The unifying theme is that of dynamic coordination variables. In leader-following, coordination is achieved through shared knowledge of the leader’s states. In the behavioral approach, coordination is achieved through shared knowledge of the relative configuration states. In the virtual structure approach, coordination is achieved through shared knowledge of the states of the virtual structure. The idea of dynamic coordination variables is similar to the notion of an “action reference” introduced in [29]. It is hoped that this paper represents a step toward a general coordination architecture that allows various control designs to be compared in a uniform framework.

The proposed hierarchical architecture is similar to hierarchical architectures that have been proposed for Intelligent Vehicle/Highway Systems [30], air traffic management [31], and an autopilot for a model helicopter [32].

The outline of this paper is as follows. In Section II, we introduce a new architecture for spacecraft formation control. We also demonstrate how the virtual structure approach to coordination can be implemented in this architecture. In Section III, we demonstrate the application of this architecture to the problem of synthesizing a deep-space, free-flying, multiple spacecraft interferometer. In particular, the following scenario will be demonstrated. A constellation of three spacecraft will first be initialized into a formation. The formation will then be retargeted to point at a star. The formation will then be controlled to cover several U–V interferometry points. A high-precision station keeping maneuver is then performed at each U–V point. Simulation results show the efficacy of the approach. Our conclusions are given in Section IV.

II. A NEW ARCHITECTURE FOR FORMATION FLYING

The objective of this section is to introduce a new architecture for spacecraft formation control that subsumes leader-following, behavioral, and virtual structure approaches and that is amenable to analysis via control theoretic methods. The general architecture is motivated by the existence of several levels of control in formation flying. At the highest level of abstraction is the dynamic transition from one subtask to another. For instance, in the interferometry scenario to be discussed in Section III, the formation must rotate to a particular pose (subtask 1), and then maintain that pose with a high level of precision (subtask 2). At the next level of abstraction, there must be a mechanism to coordinate the motion of each individual spacecraft to synthesize the desired behavior of the constellation. Finally, at the lowest level of abstraction, each individual spacecraft needs to be controlled to be consistent with the coordinating mechanism. In addition, there needs to be feedback between all three of these levels of abstraction, and this needs to be done in a way that lends itself to analysis.

A block diagram of the proposed architecture is shown schematically in Fig. 1. The system \mathcal{S}_i represents the i th

spacecraft, with control input vector \mathbf{u}_i representing control forces and torques, and output vector \mathbf{y}_i representing the measurable output of the spacecraft, most likely position and attitude vectors.

The system \mathcal{K}_i represents the local controller for the i th spacecraft. The inputs to \mathcal{K}_i are the output of the i th spacecraft \mathbf{y}_i and the coordination variable ξ . The outputs of \mathcal{K}_i are the control vector \mathbf{u}_i , and the performance variable \mathbf{z}_i .

The system \mathcal{F} is the formation control and represents the primary coordination mechanism in the system. The formation control block outputs the coordination variable ξ which is broadcast to all spacecraft. In addition, the formation control block outputs \mathbf{z}_F , which encapsulates the performance of the formation, to the supervisor. The inputs to \mathcal{F} are the performance variables from each spacecraft \mathbf{z}_i , and the output of the supervisor \mathbf{y}_G .

The system \mathcal{G} is a discrete-event supervisor that uses the performance vector \mathbf{z}_F to determine the input to the formation control \mathbf{y}_G .

State-space representations for each subsystem can be defined as follows:

$$\mathcal{S}_i: \begin{cases} \dot{\mathbf{x}}_i = f_i(\mathbf{x}_i, \mathbf{u}_i) \\ \mathbf{y}_i = h_i(\mathbf{x}_i, \mathbf{u}_i) \end{cases} \quad (1)$$

$$\mathcal{K}_i: \begin{cases} \dot{\mathbf{x}}_{ci} = a_i(\mathbf{x}_{ci}, \mathbf{y}_i, \xi) \\ \mathbf{u}_i = b_{1i}(\mathbf{x}_{ci}, \mathbf{y}_i, \xi) \\ \mathbf{z}_i = b_{2i}(\mathbf{x}_{ci}, \mathbf{y}_i, \xi) \end{cases} \quad (2)$$

$$\mathcal{F}: \begin{cases} \dot{\mathbf{x}}_F = f_F(\mathbf{x}_F, \mathbf{y}_G, \mathbf{z}_1, \dots, \mathbf{z}_N) \\ \mathbf{z}_F = h_{1F}(\mathbf{x}_F, \mathbf{y}_G, \mathbf{z}_1, \dots, \mathbf{z}_N) \\ \xi = h_{2F}(\mathbf{x}_F, \mathbf{y}_G, \mathbf{z}_1, \dots, \mathbf{z}_N) \end{cases} \quad (3)$$

$$\mathcal{G}: \begin{cases} s_t = \phi(s_{t-}, \mathbf{z}_F) \\ \mathbf{y}_G = \varphi_1(s_t, \mathbf{z}_F) \end{cases} \quad (4)$$

where \mathbf{x}_i , \mathbf{x}_{ci} and \mathbf{x}_F evolve over continuous state spaces. The supervisor \mathcal{G} is a discrete-event dynamic system where s_t evolves over a countable set of states. The coordination of individual spacecraft is accomplished through the coordination vector ξ .

The architecture shown in Fig. 1 has several advantages that are listed below.

- It accommodates both centralized and decentralized formation control schemes. For centralized control, \mathcal{F} and \mathcal{G} are implemented at a centralized location (e.g., one of the spacecraft), and then the coordination variable ξ is broadcast to the local control loops for each spacecraft. Centralized implementation will require high-bandwidth communication. For decentralized control, each spacecraft instantiates a local copy of \mathcal{F} and \mathcal{G} . For centralized control, the spacecraft are synchronized via the combined state space for \mathcal{F} and \mathcal{G} . For decentralized control the local instantiations of \mathcal{F} and \mathcal{G} must be synchronized. This can be accomplished by 1) infrequent (low bandwidth) communication; 2) building a local observer to estimate the states of the local instantiations of \mathcal{F} and \mathcal{G} on the other spacecraft; or 3) a combination of the two.
- The architecture of Fig. 1 allows a variety of control strategies to be used for both \mathcal{F} and \mathcal{K}_i . This allows a great deal

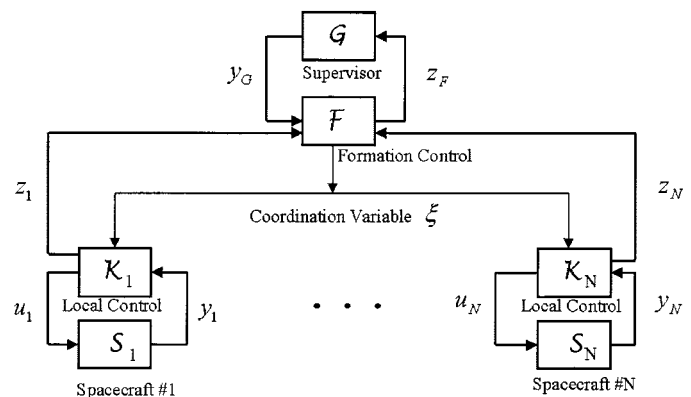


Fig. 1. Architecture for formation flying.

of flexibility in the design and analysis of formation control strategies. Essentially, the approach provides a basic architecture, allowing the objectives of the particular application to dictate the type of control used. Therefore various control designs can be studied and compared within a single framework.

- Significantly, the architecture allows feedback from the spacecraft to the coordination structure, i.e., \mathcal{F} and \mathcal{G} .
- Another advantage is that the formation dynamics \mathbf{x}_F can be propagated with a temporal advance, allowing model predictive, finite look-ahead, and feedforward control strategies at the spacecraft level. This has the potential of significantly improving the accuracy to which the formation can be maintained.
- The amount of data that must be “up-linked” from earth is fairly minimal. To initialize or reconfigure a constellation, the only thing that needs to be uploaded is at most the right-hand side of (2)–(4).
- The architecture shown in Fig. 1 is amenable to analysis via control theoretic methods.

In addition, this architecture subsumes leader-following, behavioral, and virtual structure approaches to formation control. In leader-following control, coordination is accomplished through the leading spacecraft. The formation control block is therefore the first spacecraft, with $\xi \equiv \mathbf{x}_1$. In the current literature the feedback connection from \mathcal{K}_i to \mathcal{F} has not been introduced. This is one aspect of formation control that needs to be explored.

In behavior-based control schemes, the coordination mechanism is the relative position and orientation vector of a spacecraft’s neighbors. The formation control block \mathcal{F} can be formed by stacking the relative position, velocity, attitude, and angular velocity vectors into ξ . Of course, the local control for each spacecraft only uses a subset of the elements in ξ . In currently reported behavioral schemes, interaction with a discrete-event supervisor has not been introduced. The introduction of this interaction also needs to be explored.

In the virtual structure approach, the spacecraft are coordinated through the states of the virtual structure. The remainder of this paper will focus on the application of the architecture shown in Fig. 1 in the context of the virtual structure approach. Toward that end we make the following definitions. Let \mathbf{r}_i and \mathbf{v}_i , be the inertial position and velocity of the i th spacecraft.

Also, let \mathbf{q}_i be a unit quaternion that represents the orientation of the principal axes of the i th spacecraft with respect to inertial coordinates and let $\boldsymbol{\omega}_i$ be its angular velocity. The state of the i th spacecraft is defined to be

$$\mathbf{x}_i = (\mathbf{r}'_i, \mathbf{v}'_i, \mathbf{q}'_i, \boldsymbol{\omega}'_i)'$$

and the state of the constellation is defined to be

$$\mathbf{x} = (\mathbf{x}'_1, \dots, \mathbf{x}'_N)'$$

where \mathbf{x}' is the transpose of \mathbf{x} . A superscript "d" will represent a desired quantity, e.g., \mathbf{r}_i^d is the desired inertial position of the i th spacecraft.

Conceptually, the formation can be thought of as a single "virtual" structure with inertial position \mathbf{r}_F , velocity \mathbf{v}_F , attitude \mathbf{q}_F and angular velocity $\boldsymbol{\omega}_F$. Let \mathcal{C}_F be a coordinate system located at \mathbf{r}_F with orientation given by \mathbf{q}_F , and let

$$\tilde{\mathbf{x}}_F = (\mathbf{r}'_F, \mathbf{v}'_F, \mathbf{q}'_F, \boldsymbol{\omega}'_F)'$$

The desired relative position, velocity, attitude, and angular velocity of the i th spacecraft with respect to \mathcal{C}_F is given by $\tilde{\mathbf{r}}_{iF}$, $\tilde{\mathbf{v}}_{iF}$, $\tilde{\mathbf{q}}_{iF}$, and $\tilde{\boldsymbol{\omega}}_{iF}$, respectively. Accordingly let

$$\tilde{\mathbf{x}}_{iF} = (\tilde{\mathbf{r}}'_{iF}, \tilde{\mathbf{v}}'_{iF}, \tilde{\mathbf{q}}'_{iF}, \tilde{\boldsymbol{\omega}}'_{iF})'$$

The state of the formation (also called a virtual structure in [17] and a template in [18] and [19]), is given by

$$\mathbf{x}_F = (\tilde{\mathbf{x}}'_F, \tilde{\mathbf{x}}'_{1F}, \dots, \tilde{\mathbf{x}}'_{NF})'. \quad (5)$$

If $\rho(\cdot, \cdot)$ is the geodesic metric on SO(3) as defined in Appendix A, then the distance between \mathbf{x}_i and \mathbf{x}_i^d can be defined by the following vector:

$$\hat{E}(\mathbf{x}_i, \mathbf{x}_i^d) = (\|\mathbf{r}_i - \mathbf{r}_i^d\|, \|\mathbf{v}_i - \mathbf{v}_i^d\|, \rho(\mathbf{q}_i, \mathbf{q}_i^d), \|\boldsymbol{\omega}_i - \boldsymbol{\omega}_i^d\|)'$$

Accordingly, $\|\hat{E}(\mathbf{x}_i, \mathbf{x}_i^d)\|$ is a metric that quantifies the distance between \mathbf{x}_i , and \mathbf{x}_i^d . Let

$$E(\mathbf{x}, \mathbf{x}^d) = (\hat{E}(\mathbf{x}_1, \mathbf{x}_1^d)', \dots, \hat{E}(\mathbf{x}_N, \mathbf{x}_N^d)')'$$

then $\|E(\mathbf{x}, \mathbf{x}^d)\|$ is a metric that quantifies the distance between the states of the constellation \mathbf{x} , and the desired states of the constellation \mathbf{x}^d . Note that $\|E(\cdot, \cdot)\|$ does not define a norm since $\rho(\cdot, \cdot)$ is not a norm. Similarly, the distance between the formation states \mathbf{x}_F and desired formation states \mathbf{x}_F^d is given by the metric $\|E_F(\mathbf{x}_F, \mathbf{x}_F^d)\|$, where

$$E_F(\mathbf{x}_F, \mathbf{x}_F^d) = (\hat{E}(\tilde{\mathbf{x}}_F, \tilde{\mathbf{x}}_F^d)', \hat{E}(\tilde{\mathbf{x}}_{1F}, \tilde{\mathbf{x}}_{1F}^d)', \dots, \hat{E}(\tilde{\mathbf{x}}_{NF}, \tilde{\mathbf{x}}_{NF}^d)')'$$

As illustrated by the following list, this notation can be used to naturally define a number of formation control problems.

Unconstrained Initialization. Given a fixed desired configuration \mathbf{x}^d , find $\{\mathcal{K}_i\}_{i=1}^N$ such that $\|E(\mathbf{x}(t), \mathbf{x}^d)\| \rightarrow 0$ as $t \rightarrow \infty$.

Initialization With Collision Avoidance. Given a fixed desired configuration \mathbf{x}^d , find $\{\mathcal{K}_i\}_{i=1}^N$ such that $\|E(\mathbf{x}(t), \mathbf{x}^d)\| \rightarrow 0$ as $t \rightarrow \infty$, subject to the constraint that $\|\mathbf{r}_i - \mathbf{r}_j\| > \delta$, for every $i, j = 1, \dots, N$.

Unconstrained Translation and Rotation. Suppose that the task is to translate and rotate the entire formation, as if it were a rigid body from $\mathbf{x}_F(t_0)$ to \mathbf{x}_F^d . The formation control problem is to find \mathcal{F} and $\{\mathcal{K}_i\}_{i=1}^N$ such that $\|E_F(\mathbf{x}_F(t), \mathbf{x}_F^d)\| \rightarrow 0$ and $\|E(\mathbf{x}(t), \mathbf{x}^d(t))\| \rightarrow 0$ as $t \rightarrow \infty$.

Constrained Translation and Rotation. For many applications (including the interferometry example discussed in Section III), it is desirable that the formation be translated and rotated such that certain constraints on the relative position and attitude of the spacecraft are maintained. The problem may be posed as follows. Suppose that $E(\mathbf{x}(t_0), \mathbf{x}^d(t_0)) <_e \delta$, where $<_e$ is the element-by-element inequality operator, find \mathcal{G} , \mathcal{F} and $\{\mathcal{K}_i\}$ such that $\|E_F(\mathbf{x}_F(t), \mathbf{x}_F^d)\| \rightarrow 0$ as $t \rightarrow \infty$ subject to the constraint that $E(\mathbf{x}(t), \mathbf{x}^d(t)) <_e \epsilon$, where δ and ϵ are vectors.

Attitude Constraints. A typical constraint is that the solar panels of the spacecraft need to be oriented toward the sun throughout the maneuver. This can be formulated as follows. Let \mathcal{C}_s be the coordinate frame associated with the sun, and let \mathcal{C}_p be the coordinate frame associated with the solar panel on the spacecraft which is defined such that the solar panel is perfectly aligned with the sun when the axes of \mathcal{C}_p are aligned with the axes of \mathcal{C}_s . Let \mathbf{q}_{so} represent the orientation of \mathcal{C}_s with respect to \mathcal{C}_o , and let \mathbf{q}_{io} and \mathbf{q}_{pi} be similarly defined. Then the formation control problem with sun constraints is to design \mathcal{G} , \mathcal{F} , and $\{\mathcal{K}_i\}$ such that $\|E(\mathbf{x}(t), \mathbf{x}^d(t))\| \rightarrow 0$ and $\|E_F(\mathbf{x}_F(t), \mathbf{x}_F^d)\| \rightarrow 0$ as $t \rightarrow \infty$ subject to the constraint that $\rho(\mathbf{q}_{io}, \mathbf{q}_{pi}, \mathbf{q}_{so}) < \epsilon$ (see Appendix A).

Fuel Equalization/Minimization. A critical requirement in spacecraft formation flying is to minimize the fuel expended by the spacecraft. It is also important to maintain relatively equal amounts of fuel on each of the spacecraft so that one does not run out of fuel before the others (starvation). To consider fuel optimization problems define σ_i to be the fuel mass contained on the i th spacecraft. The formation control problem under fuel constraints can be posed as follows. Find \mathcal{G} , \mathcal{F} , and $\{\mathcal{K}_i\}_{i=1}^N$ such that $\|E_F(\mathbf{x}_F, \mathbf{x}_F^d)\| \rightarrow 0$ and $\|E(\mathbf{x}, \mathbf{x}^d)\| \rightarrow 0$ as $t \rightarrow \infty$ subject to the constraint that the functional

$$\lim_{t \rightarrow \infty} \left[\sum_{i=1}^N (\sigma_i(t_0) - \sigma_i(t))^2 + \mu \sum_{i=1}^N \frac{\sigma_i(t)}{\sum_{j=1}^N \sigma_j(t)} \right] \cdot \log \left(\frac{\sigma_i(t)}{\sum_{j=1}^N \sigma_j(t)} \right)$$

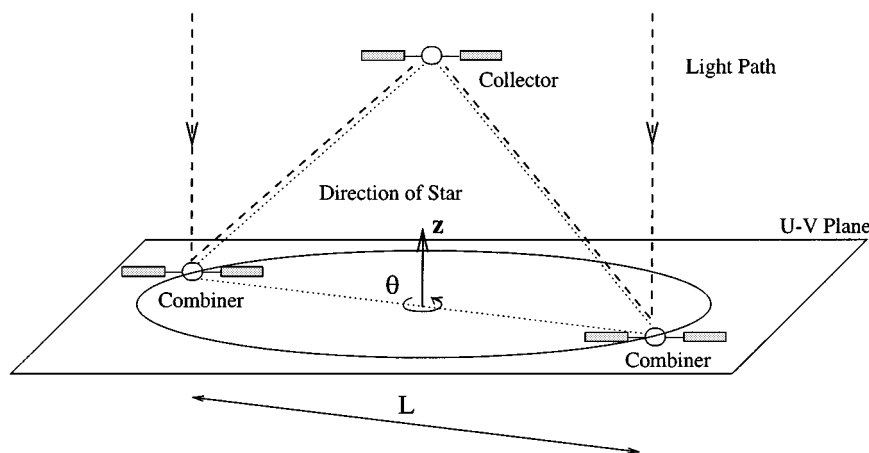


Fig. 2. Three spacecraft interferometer.

is minimized. The first term in this functional represents the total amount of fuel expended by the constellation. The second term is motivated by the negative entropy of a probability distribution [33], which is minimum for a uniform distribution, i.e., the second term will be minimized when $\lim \sigma_i(t) = \lim \sigma_j(t)$ for all $i, j \in \{1, \dots, N\}$. This objective function has been used in [28] to study fuel optimal rotations when the spacecraft are constrained to remain in formation during a maneuver, and in [27] for the case when the spacecraft are not constrained to remain in formation during the maneuver.

In the next section, we will demonstrate how these definitions are used to design a complete formation control scenario for a separated spacecraft interferometer in free space.

III. INTERFEROMETRY EXAMPLE

To fix ideas, we will give an example motivated by the New Millennium Deep Space 3 (DS3) mission currently planned by NASA for launch in 2003 [34], [35]. One instantiation of DS3 consists of three spacecraft that fly in formation in a heliocentric orbit.¹ The objective of the formation is to synthesize a space-based interferometer for imaging stars. A picture of a three spacecraft interferometer is shown in Fig. 2.

An interferometer works by collecting two light beams that have traveled different paths from the same source, and then combining the beams to create an interference fringe pattern. The width, angle and intensity of the fringe pattern determines $\mu(u, v)$ which is the mutual coherence function of the light source, where u and v are frequency variables in the Fourier domain. The intensity map, or image, of the source is obtained through an inverse Fourier transform of the mutual coherence function [36]. The mutual coherence function is parameterized by the variables u and v which range over \mathbb{R} , forming a plane called the “U–V plane.” The physical configuration of the spacecraft formation determines the particular point (u, v) in the U–V plane.

The mapping from physical space to the U–V plane is many-to-one, in fact there are an infinite number of physical configurations corresponding to a single point (u, v) . Fig. 2 shows a three spacecraft interferometer, where the spacecraft are configured in an equilateral triangle. The vector \mathbf{z} in the figure points in the direction of the light source. The distance between the two “combiner” spacecraft is called the baseline and is of length L . The angle of the baseline with respect to \mathbf{z} is denoted by θ . The physical configuration parameters (L, θ) map to a single (u, v) point (which may give more information about the image if the light source has symmetry properties). To image a star, the formation must undergo a sequence of maneuvers that correspond to a sequence of baseline-angle pairs (L_i, θ_i) . At each baseline-angle pair, the entire formation must pose and collect light. During the collection process, the relative distance between the spacecraft must be precisely controlled with errors on the order of nanometers (accomplished through three stages of control including micro-thrusters on the spacecraft, voice-coil actuation on the carts holding the mirrors, and piezoelectric actuation of the mirrors).

To accomplish an interferometry mission, the formation will have several modes of operation.

Mode 1. First, the constellation must be initialized into a desired formation pattern, e.g., an equilateral triangle.

Mode 2. Second, the formation must be maneuvered such that the vector \mathbf{z} points in the direction of the light source to be imaged, ℓ_i .

Mode 3. Third the formation pattern needs to be rotated and stretched to correspond to a particular baseline-angle pair (L_i, θ_i) .

Mode 4. Fourth, high gain feedback needs to be used to very accurately position the spacecraft to prepare for light collection at (L_i, θ_i) .

Mode 5. Finally, the control loop involving the thrusters is turned off and light is collected for a fixed period of time.

Modes four and five may need to be repeated several times if the spacecraft drift outside an acceptable range during the light collection phase. Each mode of operation will correspond to a different control strategy. We will now show how a control

¹The current approach is to use two spacecraft instead of three.

system for this mission can be designed and analyzed using the architecture introduced in Section II.

A. Spacecraft Dynamics

Before designing the control laws for each mode of operation, it is necessary to obtain the dynamic model for each spacecraft, i.e., to specify \mathcal{S}_i in Fig. 1. Each spacecraft will be modeled as a rigid body, with \mathbf{r}_i , \mathbf{v}_i , \mathbf{q}_i , and $\boldsymbol{\omega}_i$ representing the position, velocity, unit attitude quaternion, and angular velocity of the i th spacecraft. The dynamic equations of motion are given by the following equations [37]:

$$\begin{aligned} \dot{\mathbf{r}}_i &= \mathbf{v}_i \\ \mathbf{M}_i \dot{\mathbf{v}}_i &= \mathbf{f}_i \\ \dot{\mathbf{q}}_i &= -\frac{1}{2} \boldsymbol{\omega}_i \times \mathbf{q}_i + \frac{1}{2} \bar{q}_i \boldsymbol{\omega}_i \\ \dot{\bar{q}}_i &= -\frac{1}{2} \boldsymbol{\omega}_i \cdot \mathbf{q}_i \\ \mathbf{J}_i \dot{\boldsymbol{\omega}}_i &= -\mathbf{J}_i \boldsymbol{\omega}_i \times \boldsymbol{\omega}_i + \boldsymbol{\tau}_i \end{aligned} \quad (6)$$

where

- \mathbf{M}_i and \mathbf{J}_i mass and inertia of the i th spacecraft, respectively;
- \mathbf{q} vector part of the quaternion \mathbf{q} ;
- \bar{q} scalar part of the quaternion \mathbf{q} (see Appendix A);
- \mathbf{f}_i control force;
- $\boldsymbol{\tau}_i$ control torque on the i th spacecraft.

The vector \mathbf{x}_i and \mathbf{u}_i specified in (1) are therefore defined by $\mathbf{x}_i = (\mathbf{r}'_i, \mathbf{v}'_i, \mathbf{q}'_i, \boldsymbol{\omega}'_i)$, and $\mathbf{u}_i = (\mathbf{f}'_i, \boldsymbol{\tau}'_i)$, respectively. The vector field f_i is defined by (6). Throughout this paper, we will assume that $\mathbf{y}_i = \mathbf{x}_i$, i.e., that all of the spacecraft states are available for feedback.

The formation control will be derived by first specifying \mathcal{G} , then \mathcal{F} and then finally $\{\mathcal{K}_i\}_{i=1}^N$.

B. Supervisor

A state diagram for an interferometry mission is shown in Fig. 3, where

$$\begin{aligned} G1 &= \begin{cases} \text{True;} & \|E(\mathbf{x}, \mathbf{x}^d)\| < \epsilon_1 \\ \text{False;} & \text{otherwise} \end{cases} \\ G2 &= \begin{cases} \text{True;} & \|E(\mathbf{x}, \mathbf{x}^d)\| < \epsilon_2, \text{ and} \\ & \|E_F(\mathbf{x}_F, \mathbf{x}_F^d)\| < \epsilon_3 \\ \text{False;} & \text{otherwise} \end{cases} \\ G3 &= \begin{cases} \text{True;} & \|E(\mathbf{x}, \mathbf{x}^d)\| < \epsilon_4, \text{ and} \\ & \|E_F(\mathbf{x}_F, \mathbf{x}_F^d)\| < \epsilon_5 \\ \text{False;} & \text{otherwise} \end{cases} \\ G4 &= \begin{cases} \text{True;} & \|E(\mathbf{x}, \mathbf{x}^d)\| < \epsilon_6 \text{ and} \\ & \|E_F(\mathbf{x}_F, \mathbf{x}_F^d)\| < \epsilon_7 \\ \text{False;} & \text{otherwise} \end{cases} \\ G5 &= \begin{cases} \text{True;} & t - t_0 \leq T, \text{ and either} \\ & \|E(\mathbf{x}, \mathbf{x}^d)\| \geq \epsilon_8, \text{ or} \\ & \|E_F(\mathbf{x}_F, \mathbf{x}_F^d)\| \geq \epsilon_9 \\ \text{False;} & \text{otherwise} \end{cases} \\ G6 &= \begin{cases} \text{True;} & t - t_0 > T \\ \text{False;} & \text{otherwise.} \end{cases} \end{aligned}$$

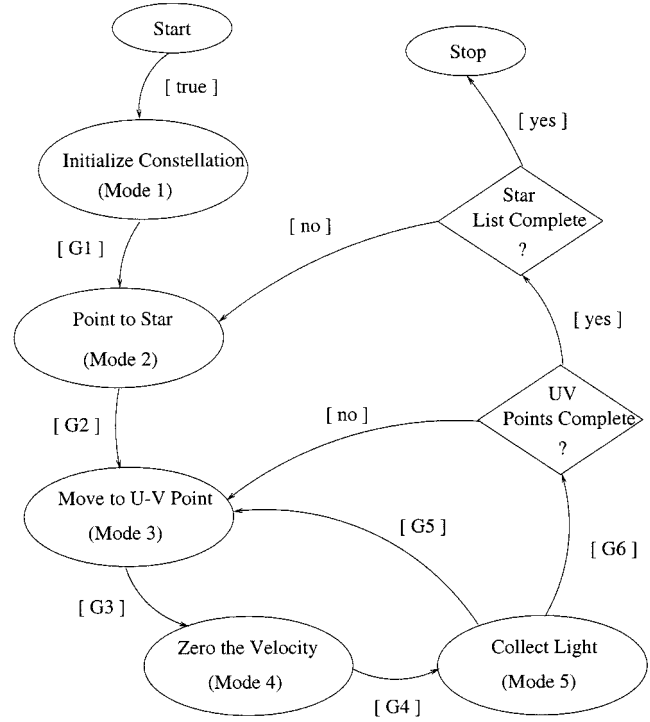


Fig. 3. State diagram of the supervisor \mathcal{G} .

The states of the diagram correspond to the modes of operation listed above. In each state, a different control law will be used for the spacecraft. The block diagram outlines the basic structure of the supervisor \mathcal{G} . As shown in Fig. 1, the output of the supervisor is the input to the formation control block \mathbf{y}_G . This vector will be composed of three elements: 1) an index (j) that specifies the low-level control to be used; 2) and index (k) indicating the formation dynamics to be used; and 3) additional data specifying, for example, target configurations for the formation. The output for each mode of operation is as follows:

Mode 1. $\mathbf{y}_G = (j = 1, k = 1, \mathbf{x}^d)'$, where \mathbf{x}^d is the desired position and orientation of each of the spacecraft within the initial formation.

Mode 2. $\mathbf{y}_G = (j = 2, k = 2, \mathbf{q}_F^d)'$, where \mathbf{q}_F^d is a quaternion specifying desired formation attitude required to point at the next star on a predefined list.

Mode 3. $\mathbf{y}_G = (j = 2, k = 3, L_i, \theta_i)'$, where (L_i, θ_i) is the next desired U-V point of the mutual coherence function. For each star, it is assumed that there is a predefined list of pairs (L_i, θ_i) .

Mode 4. $\mathbf{y}_G = (j = 3, k = 4)'$.

Mode 5. $\mathbf{y}_G = (j = 4, k = 4)'$.

From the specification of the state flow diagram, it is straightforward to put the supervisor in the form of (4).

C. Formation Control

In this section we will design the formation control block \mathcal{F} . As can be seen from the above discussion, \mathcal{F} is a hybrid system with three modes of operation.

The development of \mathcal{F} and \mathcal{K}_i will depend on the following lemma.

Lemma 1: Let $\hat{\mathbf{x}} = (\mathbf{r}', \mathbf{v}', \mathbf{q}', \boldsymbol{\omega}')'$, $\hat{\mathbf{x}}^d = (\mathbf{r}^d, \mathbf{v}^d, \mathbf{q}^d, \boldsymbol{\omega}^d)'$, $\mathbf{M} > 0$ be the mass of the spacecraft, $\mathbf{J} = \mathbf{J}' > 0$ be the inertia, and let

$$\begin{aligned} \dot{\hat{\mathbf{x}}} &= f_c(\hat{\mathbf{x}}) + g_c(\hat{\mathbf{x}}, \hat{\mathbf{x}}^d, \ell) \\ &\triangleq \begin{pmatrix} \mathbf{v} \\ \mathbf{0} \\ \frac{1}{2} \Omega(\boldsymbol{\omega}) \mathbf{q} \\ -\boldsymbol{\omega} \times \mathbf{J} \boldsymbol{\omega} \end{pmatrix} + \begin{pmatrix} \mathbf{0} \\ -K_r^{(\ell)}(\mathbf{r} - \mathbf{r}^d) - K_v^{(\ell)}(\mathbf{v} - \mathbf{v}^d) \\ \mathbf{0} \\ K_q^{(\ell)} \tilde{\mathbf{q}}_e - K_\omega^{(\ell)}(\boldsymbol{\omega} - \boldsymbol{\omega}^d) \end{pmatrix} \end{aligned}$$

where $\tilde{\mathbf{q}}_e = \mathbf{q}^* \mathbf{q}^d$. Also let

$$\hat{E}(\hat{\mathbf{x}}, \hat{\mathbf{x}}^d) = (\|\mathbf{r} - \mathbf{r}^d\|, \|\mathbf{v} - \mathbf{v}^d\|, \rho(\mathbf{q}, \mathbf{q}^d), \|\boldsymbol{\omega} - \boldsymbol{\omega}^d\|)'$$

If

- 1) $K_r^{(\ell)} = K_r^{(\ell)'} > 0$, $K_v^{(\ell)} = K_v^{(\ell)'} > 0$, $K_q^{(\ell)} = K_q^{(\ell)'} > 0$, $K_\omega^{(\ell)} = K_\omega^{(\ell)'} > 0$;
- 2) $\ddot{\mathbf{r}}^d \in L_2[0, \infty) \cap L_\infty[0, \infty)$;
- 3) $\|\dot{\boldsymbol{\omega}}^d\| + \|\boldsymbol{\omega}^d\|^2 \in L_2[0, \infty) \cap L_\infty[0, \infty)$;

then $\|\hat{E}(\hat{\mathbf{x}}, \hat{\mathbf{x}}^d)\| \rightarrow 0$ as $t \rightarrow \infty$.

Proof: See Appendix B.

Lemma 1 delimits the class of trajectories that can be tracked using the controls outlined in this paper. In particular, the acceleration of the translational trajectories must be bounded and have finite energy. Alternatively, for rotational trajectories, we require that both the trajectory and its velocity be bounded with finite energy.

Note that Lemma 1 implies a PD-like control strategy, which will be used to control both the formation and each individual spacecraft. The choice of PD control is simply illustrative. Any control strategy that guarantees that the system transitions out of the states shown in Fig. 3 could also have been used.

The dynamic equations for \mathcal{F} are given by (3), where $\mathbf{z}_i = \mathbf{x}_i$ and where \mathbf{x}_F is given by (5).

1) *Mode 1—Initialization:* During the initialization mode, the output of the supervisor is $\mathbf{y}_G = (j = 1, k = 1, \mathbf{x}^d)'$, where $j = 1$ indicates that the first low-level control law should be used, $k = 1$ indicates that the first formation control strategy should be used and \mathbf{x}^d is the desired position and orientation of each of the spacecraft within the initial formation, i.e.,

$$\mathbf{x}^d = (\mathbf{r}_1^{d'}, \mathbf{0}', \mathbf{q}_1^{d'}, \mathbf{0}', \dots, \mathbf{r}_N^{d'}, \mathbf{0}', \mathbf{q}_N^{d'}, \mathbf{0}')'$$

The desired position and attitude for each spacecraft will simply be passed directly to the local control for each spacecraft (i.e., \mathcal{K}_i), in other words

$$\boldsymbol{\xi} = h_{2F}(\mathbf{x}_F, \mathbf{y}_G, \mathbf{z}_1, \dots, \mathbf{z}_N) \triangleq (j = 1, \mathbf{x}^d)'$$

The objective of f_F when $k = 1$, will be to initialize \mathbf{r}_F to the geometric center of the formation, with an orientation identical to the inertial frame, i.e., we let

$$\begin{aligned} \mathbf{x}_F^d(\mathbf{x}^d) &= \left(\frac{1}{N} \sum_{i=1}^N \mathbf{r}_i^{d'}, \mathbf{0}', \mathbf{q}_1^{d'}, \mathbf{0}', \mathbf{r}_1^{d'} - \frac{1}{N} \sum_{i=1}^N \mathbf{r}_i^{d'}, \mathbf{0}', \mathbf{q}_i^{d'}, \right. \\ &\quad \left. \mathbf{0}', \dots, \mathbf{r}_N^{d'} - \frac{1}{N} \sum_{i=1}^N \mathbf{r}_i^{d'}, \mathbf{0}', \mathbf{q}_N^{d'}, \mathbf{0}' \right)' \\ &\triangleq (\tilde{\mathbf{x}}_F^{d'}, \tilde{\mathbf{x}}_{1F}^{d'}, \dots, \tilde{\mathbf{x}}_{NF}^{d'})' \end{aligned}$$

The formation dynamics for the initialization mode are given by

$$\begin{aligned} \dot{\mathbf{x}}_F &= f_F(\mathbf{x}_F, \mathbf{y}_G, \mathbf{z}_1, \dots, \mathbf{z}_N) \\ &\triangleq \begin{pmatrix} f_c(\tilde{\mathbf{x}}_F) + g_c(\tilde{\mathbf{x}}_F, \tilde{\mathbf{x}}_F^d, k = 1) \\ f_c(\tilde{\mathbf{x}}_{1F}) + g_c(\tilde{\mathbf{x}}_{1F}, \tilde{\mathbf{x}}_{1F}^d, k = 1) \\ \vdots \\ f_c(\tilde{\mathbf{x}}_{NF}) + g_c(\tilde{\mathbf{x}}_{NF}, \tilde{\mathbf{x}}_{NF}^d, k = 1) \end{pmatrix}. \end{aligned}$$

Since the purpose of f_F when $k = 1$ is to align the formation states with the initialized formation, the control gains $K_r^{(1)}$, $K_v^{(1)}$, $K_q^{(1)}$, and $K_\omega^{(1)}$ can be chosen to make the formation state converge very quickly.

The performance variable \mathbf{z}_F associated with \mathcal{F} in this mode is

$$\mathbf{z}_F = h_{1F}(\mathbf{x}_F, \mathbf{y}_G, \mathbf{z}_1, \dots, \mathbf{z}_N) \triangleq E_F(\mathbf{x}_F, \mathbf{x}_F^d(\mathbf{x}^d)).$$

2) *Mode 2—Point to Star:* In the point-to-star mode, the output of the supervisor is $\mathbf{y}_G = (j = 2, k = 2, \mathbf{q}_F^d)'$, where $j = 2$ indicates that the second low-level control law should be used, $k = 1$ indicates that the first formation control strategy should be used, and where \mathbf{q}_F^d is a unit quaternion representing the orientation, in inertial coordinates, of the next star on a predefined list. When $k = 2$, the coordination variable is

$$\boldsymbol{\xi} = h_{2F}(\mathbf{x}_F, \mathbf{y}_G, \mathbf{z}_1, \dots, \mathbf{z}_N) \triangleq (j = 2, \mathbf{x}'_F)'$$

In this mode, the objective of f_F is to reorient the formation to the desired orientation \mathbf{q}_F^d . Accordingly, we let

$$\begin{aligned} \mathbf{x}_F^d(\mathbf{q}_F^d, \mathbf{x}_F(t_0)) &= (\mathbf{r}_F(t_0)', \mathbf{v}_F(t_0)', \mathbf{q}_F^{d'}, \mathbf{0}', \tilde{\mathbf{r}}_{1F}(t_0)', \\ &\quad \tilde{\mathbf{v}}_{1F}(t_0)', \tilde{\mathbf{q}}_{1F}(t_0)', \tilde{\boldsymbol{\omega}}_{1F}(t_0)', \dots, \\ &\quad \tilde{\mathbf{r}}_{3F}(t_0)', \tilde{\mathbf{v}}_{3F}(t_0)', \tilde{\mathbf{q}}_{3F}(t_0)', \tilde{\boldsymbol{\omega}}_{3F}(t_0)')' \\ &\triangleq (\tilde{\mathbf{x}}_F^{d'}, \tilde{\mathbf{x}}_{1F}^{d'}, \dots, \tilde{\mathbf{x}}_{3F}^{d'})' \end{aligned}$$

where t_0 is the last time at which the supervisor entered mode 2, and let

$$\begin{aligned} \dot{\mathbf{x}}_F &= f_F(\mathbf{x}_F, \mathbf{y}_G, \mathbf{z}_1, \dots, \mathbf{z}_N) \\ &\triangleq \begin{pmatrix} f_c(\tilde{\mathbf{x}}_F) + g_c(\tilde{\mathbf{x}}_F, \tilde{\mathbf{x}}_F^d, k = 2) \\ f_c(\tilde{\mathbf{x}}_{1F}) + g_c(\tilde{\mathbf{x}}_{1F}, \tilde{\mathbf{x}}_{1F}^d, k = 2) \\ \vdots \\ f_c(\tilde{\mathbf{x}}_{NF}) + g_c(\tilde{\mathbf{x}}_{NF}, \tilde{\mathbf{x}}_{NF}^d, k = 2) \end{pmatrix}. \end{aligned}$$

Note that the gain matrices $K_q^{(2)}$ and $K_\omega^{(2)}$ determine the rate at which the entire formation is reoriented to the new star location. In general it is desirable that these gains be about an order of magnitude slower than the position and attitude gains for the local spacecraft controls.

The performance variable \mathbf{z}_F associated with this mode is

$$\begin{aligned} \mathbf{z}_F &= h_{1F}^{(2)}(\mathbf{x}_F, \mathbf{y}_G, \mathbf{z}_1, \dots, \mathbf{z}_N) \\ &\triangleq E_F(\mathbf{x}_F(t), \mathbf{x}_F^d(\mathbf{q}_F^d, \mathbf{x}_F(t_0))). \end{aligned}$$

3) *Mode 3—Move to U-V Point:* During the move to U-V point mode, the output of the supervisor is $\mathbf{y}_G = (j = 2, k = 3, L_i, \theta_i)'$, where $j = 2$ indicates that the same low-level control law is used in Mode 3 as was used in Mode 2, $k = 3$ indicates that the third formation control strategy is used, and (L_i, θ_i) are the baseline and boresight rotation angle associated

with the next desired U–V point of the mutual coherence function. The coordination variable associated with this mode is

$$\xi = h_{2F}(\mathbf{x}_F, \mathbf{y}_G, \mathbf{z}_1, \dots, \mathbf{z}_N) \triangleq (j = 2, x^d)'$$

There are two objectives associated with f_F for the move to U–V point mode: 1) Expand the formation to match the baseline L_i , 2) Rotate the formation about its boresight to the angle θ_i . Suppose that the initial orientation of the formation is such that the boresight of the formation is initially aligned along the \mathbf{z} axis of C_0 , and that the unit quaternion \mathbf{q}_{1F}^d represents the rotation required to align the boresight in the direction of the desired star. Then, according to Appendix A, a rotation of angle θ_i about the boresight of the interferometer is given by

$$\tilde{\mathbf{q}}_i = \left(0, 0, \sin\left(\frac{\theta_i}{2}\right), \cos\left(\frac{\theta_i}{2}\right) \right)' \mathbf{q}_{1F}^d.$$

Let C_F be aligned with the interferometer as shown in Fig. 4. Then the desired positions of the spacecraft with respect to C_F are

$$\begin{aligned} \tilde{\mathbf{r}}_{1F}^i &= (0, 0, L_i)' \\ \tilde{\mathbf{r}}_{2F}^i &= (L_i/2, 0, 0)' \\ \tilde{\mathbf{r}}_{3F}^i &= (-L_i/2, 0, 0)' \end{aligned}$$

Accordingly, let

$$\begin{aligned} \mathbf{x}_F^d(L_i, \theta_i) &= (\mathbf{r}_F(t_0)', \mathbf{v}_F(t_0)', \tilde{\mathbf{q}}_i', \mathbf{0}', \tilde{\mathbf{r}}_{1F}^i', \mathbf{0}', \tilde{\mathbf{q}}_{1F}(t_0)' \\ &\quad \mathbf{0}', \dots, \tilde{\mathbf{r}}_{3F}^i', \mathbf{0}', \tilde{\mathbf{q}}_{3F}(t_0)', \mathbf{0}')' \\ &\triangleq (\tilde{\mathbf{x}}_F^d', \tilde{\mathbf{x}}_{1F}^d', \tilde{\mathbf{x}}_{2F}^d', \tilde{\mathbf{x}}_{3F}^d')' \end{aligned}$$

where t_0 is the last time at which the supervisor entered Mode 3. In addition, let

$$\dot{\mathbf{x}}_F = f_F(\mathbf{x}_F, \mathbf{y}_G, \mathbf{z}_1, \dots, \mathbf{z}_N) \triangleq \begin{pmatrix} f_c(\tilde{\mathbf{x}}_F) + g_c(\tilde{\mathbf{x}}_F, \tilde{\mathbf{x}}_F^d, k = 3) \\ f_c(\tilde{\mathbf{x}}_{1F}) + g_c(\tilde{\mathbf{x}}_{1F}, \tilde{\mathbf{x}}_{1F}^d, k = 3) \\ \vdots \\ f_c(\tilde{\mathbf{x}}_{NF}) + g_c(\tilde{\mathbf{x}}_{NF}, \tilde{\mathbf{x}}_{NF}^d, k = 3) \end{pmatrix}.$$

Note that the gain matrices $K_q^{(3)}$ and $K_\omega^{(3)}$ determine the rate at which the entire formation is rotated to the new angle θ_i and that $K_r^{(3)}$ and $K_v^{(3)}$ determine the rate at which the entire formation expands or contracts to the new baseline L_i . In general these gains should be about an order of magnitude slower than the control gains for the local spacecraft control.

The performance variable \mathbf{z}_F associated with this mode is

$$\mathbf{z}_F = h_{1F}(\mathbf{x}_F, \mathbf{y}_G, \mathbf{z}_1, \dots, \mathbf{z}_N) \triangleq E_F(\mathbf{x}_F(t), \mathbf{x}_F^d(L_i, \theta_i)).$$

4) *Mode 4—Zero the Velocity*: For the zero-the-velocity mode the output of the supervisor is $\mathbf{y}_G = (j = 3, k = 4)$ indicating that the third low-level control law and the fourth formation control strategy are to be used. Similar to the previous two modes, the coordination variable in this mode is

$$\xi = (j = 3, \mathbf{x}_F)'$$

The objective of f_F in this mode is to apply high gain feedback to increase the precision of the current pose of the formation. Accordingly, the desired state of the formation is its state at the

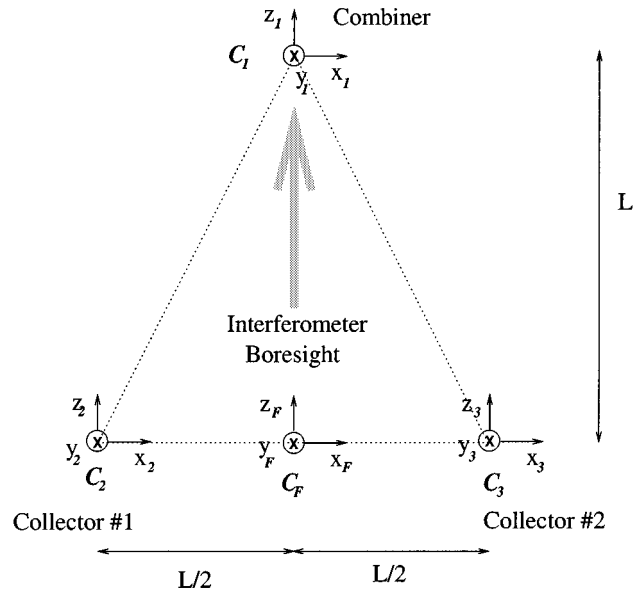


Fig. 4. The coordinate alignment of the interferometer.

time that Mode 4 is entered, i.e., $\mathbf{x}_F^d = \mathbf{x}_F(t_0)$ where t_0 is the last time at which the supervisor entered Mode 4. Accordingly, the formation dynamics in Mode 4 are

$$\dot{\mathbf{x}}_F = f_F(\mathbf{x}_F, \mathbf{y}_G, \mathbf{z}_1, \dots, \mathbf{z}_N) \triangleq \begin{pmatrix} f_c(\tilde{\mathbf{x}}_F) + g_c(\tilde{\mathbf{x}}_F, \tilde{\mathbf{x}}_F^d, k = 4) \\ f_c(\tilde{\mathbf{x}}_{1F}) + g_c(\tilde{\mathbf{x}}_{1F}, \tilde{\mathbf{x}}_{1F}^d, k = 4) \\ \vdots \\ f_c(\tilde{\mathbf{x}}_{NF}) + g_c(\tilde{\mathbf{x}}_{NF}, \tilde{\mathbf{x}}_{NF}^d, k = 4) \end{pmatrix} \quad (7)$$

where $K_r^{(4)}$, $K_v^{(4)}$, $K_q^{(4)}$, and $K_\omega^{(4)}$ are selected to provide high gain feedback on the formation states.

The performance variable \mathbf{z}_F associated with this mode is

$$\mathbf{z}_F = h_{1F}(\mathbf{x}_F, \mathbf{y}_G, \mathbf{z}_1, \dots, \mathbf{z}_N) \triangleq E_F(\mathbf{x}_F(t), \mathbf{x}_F(t_0)). \quad (8)$$

5) *Mode 5—Collect Light*: In the collect light mode the output of the supervisor is $\mathbf{y}_G = (j = 4, k = 4)$ indicating that the fourth low-level control law and the fourth formation control strategy should be applied. The objective of this mode is to turn off the thrusters so that interferometric data can be collected without interference from the thrusters. Therefore the local controls will be set to zero. However, it is important to measure the deviation of the spacecraft from the desired formation, so that if the interferometer drifts out of alignment, light collection can be interrupted to realign the formation.

Similar to the previous three modes, the coordination variable is

$$\xi = (j = 4, \mathbf{x}_F)$$

where the formation state \mathbf{x}_F can be kept in its current configuration through application of the same formation strategy used in Mode 4. Accordingly, the formation dynamics for Mode 5 are given by (7). Note that in the next section, the gains for the local feedback in Mode 5 will be set to zero. Therefore, the desired

formation remains fixed, but the spacecraft may not track the formation.

The performance variable \mathbf{z}_F associated with this mode is given by (8).

D. Local Controls

Next we design a local control law $\{\mathcal{K}_i\}$ for each mode of operation listed above. The form of the local control will be identical for each mode of operation, however the gains will be different. When the constellation is in Mode 4, high gain feedback is desired to maintain very precise relative position and attitude constraints. In Mode 1 however, low gain feedback is required to avoid actuator saturation and unnecessary motion in the spacecraft. Modes 2 and 3 required intermediate gains. The gains in Mode 5 are set to zero.

1) *Mode 1—Initialization:* The local control for Mode 1 is straightforward. The state-space equations for \mathcal{K}_i have the form

$$\begin{aligned}\dot{\boldsymbol{\xi}}_i &= a_i(\boldsymbol{\xi}_i, \mathbf{x}_i, \mathbf{y}_F, j) \\ \mathbf{u}_i &= b_i(\boldsymbol{\xi}_i, \mathbf{x}_i, \mathbf{y}_F, j)\end{aligned}$$

where in this case $\boldsymbol{\xi} = (j = 1, \mathbf{x}^d)'$. Therefore we let $a_i(\boldsymbol{\xi}_i, \mathbf{x}_i, P_i(\mathbf{x}^d), 1) = 0$ and $b_i(\mathbf{x}_i, P_i(\mathbf{x}^d), 1) = g_c(\mathbf{x}_i, \mathbf{x}_i^d, 5)$, where $P_i(\mathbf{x}^d) \triangleq \mathbf{x}_i^d$ and where $K_r^{(5)}$, $K_v^{(5)}$, $K_q^{(5)}$, and $K_\omega^{(5)}$ are chosen to give the spacecraft relatively slow dynamics.

2) *Mode 2, 3 and 4:* For Modes 2, 3, and 4 the output of \mathcal{F} is $\boldsymbol{\xi} = (j, \mathbf{x}_F)'$. To use Lemma 1 we need to map $\mathbf{x}_F(t)$ to $\mathbf{x}_i^d(t)$ for each $i = 1, \dots, N$. The transformation is derived by considering the coordinate geometry shown in Fig. 5. The desired transformation is given by (cf. [38])

$$\mathbf{x}_i^d = T_i(\mathbf{x}_F) \triangleq \begin{pmatrix} \mathbf{r}_F + \tilde{\mathbf{r}}_{iF} \\ \mathbf{v}_F + \tilde{\mathbf{v}}_{iF} + \boldsymbol{\omega}_F \times \tilde{\mathbf{r}}_{iF} \\ \tilde{\mathbf{q}}_{iF} \mathbf{q}_F \\ \boldsymbol{\omega}_F + \tilde{\boldsymbol{\omega}}_{iF} \end{pmatrix}.$$

Therefore the control laws for Modes 2 and 3 are given by $a_i(\mathbf{x}_i, T_i(\mathbf{x}^d), 2) = 0$ and $b_i(\mathbf{x}_i, T_i(\mathbf{x}^d), 2) = g_c(\mathbf{x}_i, \mathbf{x}_i^d, 6)$, where the gains $\{K_r^{(6)}, K_v^{(6)}, K_q^{(6)}, K_\omega^{(6)}\}$ are chosen to be about an order of magnitude greater than both $\{K_r^{(2)}, K_v^{(2)}, K_q^{(2)}, K_\omega^{(2)}\}$ and $\{K_r^{(3)}, K_v^{(3)}, K_q^{(3)}, K_\omega^{(3)}\}$. Similarly, the control laws for Mode 4 are given by $a_i(\mathbf{x}_i, T_i(\mathbf{x}^d), 3) = 0$ and $b_i(\mathbf{x}_i, T_i(\mathbf{x}^d), 3) = g_c(\mathbf{x}_i, \mathbf{x}_i^d, 7)$, where the gains $\{K_r^{(7)}, K_v^{(7)}, K_q^{(7)}, K_\omega^{(7)}\}$ are chosen to be about an order of magnitude greater than $\{K_r^{(4)}, K_v^{(4)}, K_q^{(4)}, K_\omega^{(4)}\}$.

3) *Mode 5:* In Mode 5, the feedback gains are set to zero to eliminate the local feedback to the spacecraft.

E. Analysis

In the absence of disturbances, the analysis for this system is straightforward. We would like to ensure that given an initial state for the constellation $\mathbf{x}(t_0)$, if the Supervisor begins in the ‘‘START’’ state as shown in Fig. 3, that it will reach the ‘‘STOP’’ state in a finite amount of time. An obvious necessary condition for this to be true is that the list of stars and the list of U–V points for each star is finite. In the absence of disturbances the Mode 3–Mode 4–Mode 5 loop will be executed at most once. In which

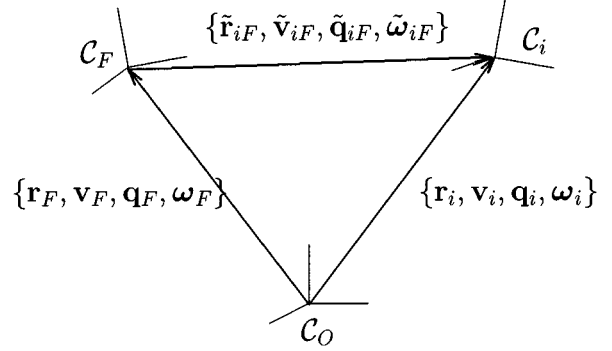


Fig. 5. Coordinate frame geometry.

case, it is sufficient to argue that the transition out of Modes 1, 2, 3, and 4 always occur in a finite amount of time, but this is ensured by Lemma 1 and the construction of \mathcal{F} and \mathcal{K}_i .

In reality common space disturbances will be present. When disturbances are present, the low-level controllers need to be designed to reject these disturbances such that the transitions out of Modes 1, 2, 3, and 4 always occur and such that the Mode 3–Mode 4–Mode 5 loop is guaranteed to execute a finite number of times.

F. Simulation Results

Simulations were written in MATLAB, Simulink, and Stateflow. To show the dynamic behavior of the spacecraft, we will show position and attitude error plots for the combiner. We will also show the relative position and attitude errors of the combiner with respect to the collectors. Fig. 6 shows error plots for Mode 1. Fig. 7 shows error plots for the transition from Mode 1 to Mode 2. Fig. 8 shows error plots for the transition from Mode 2 to Mode 3. Finally, Fig. 9 shows error plots for the transition from Mode 3 to Mode 4.

Note that the gains of the control scheme listed above have been tuned for suitable transient response of the formation errors. They have not, however, been tuned to minimize fuel usage and execution time for the maneuvers. The lifespan of deep space interferometry missions will be a function of the fuel on-board the spacecraft, therefore fuel minimization is a critical component. In addition to fuel minimization it is desirable that one spacecraft does not run out of fuel before the others. Of course a small amount of fuel is need to terminate the existence of each satellite as part of the flight protocol, thus the coordination problem cannot completely deplete the available fuel. The problem of maintaining equal amounts of fuel on each spacecraft is called fuel equalization. The architecture introduced in Fig. 1 can be used to design fuel minimizing/equalizing maneuvers for spacecraft formations. In [28] and [39] we have used this architecture to design fuel equalizing/maneuvers when the spacecraft are required to maintain formation throughout the maneuver. In [27] and [40] we use similar techniques to solve the fuel equalization/minimization problem when the spacecraft are allowed to break formation during the maneuver.

IV. CONCLUSION

In this paper, we have introduced a new architecture for spacecraft formation flying and demonstrated the application of this

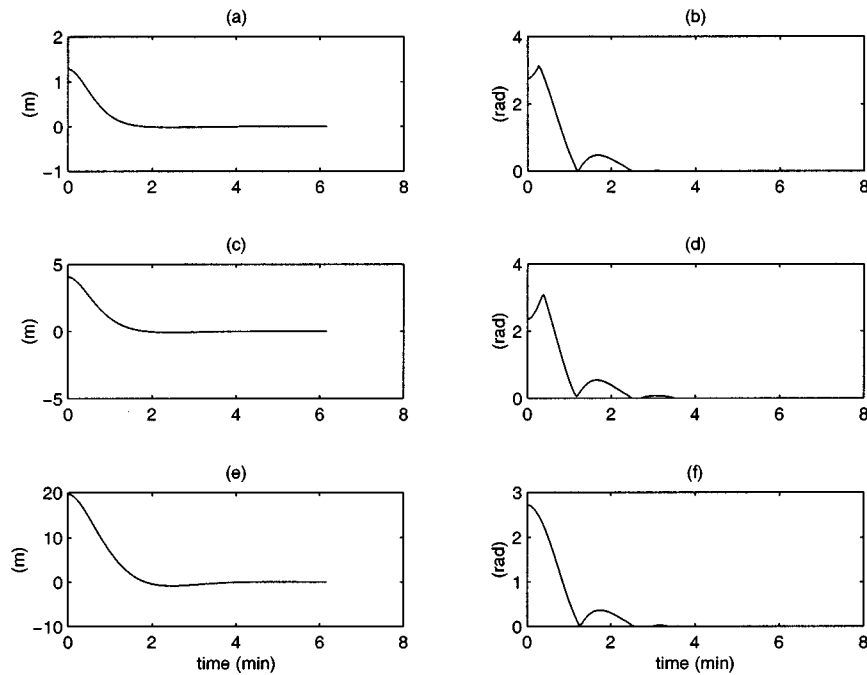


Fig. 6. Position and attitude errors in Mode 1. (a) Absolute position error for spacecraft #1. (b) Absolute attitude error for Spacecraft #1. (c) Relative position error between Spacecraft #1 and #2. (d) Relative attitude error between Spacecraft #1 and #2. (e) Relative position error between Spacecraft #1 and #3. (f) Relative attitude error between Spacecraft #1 and #3.

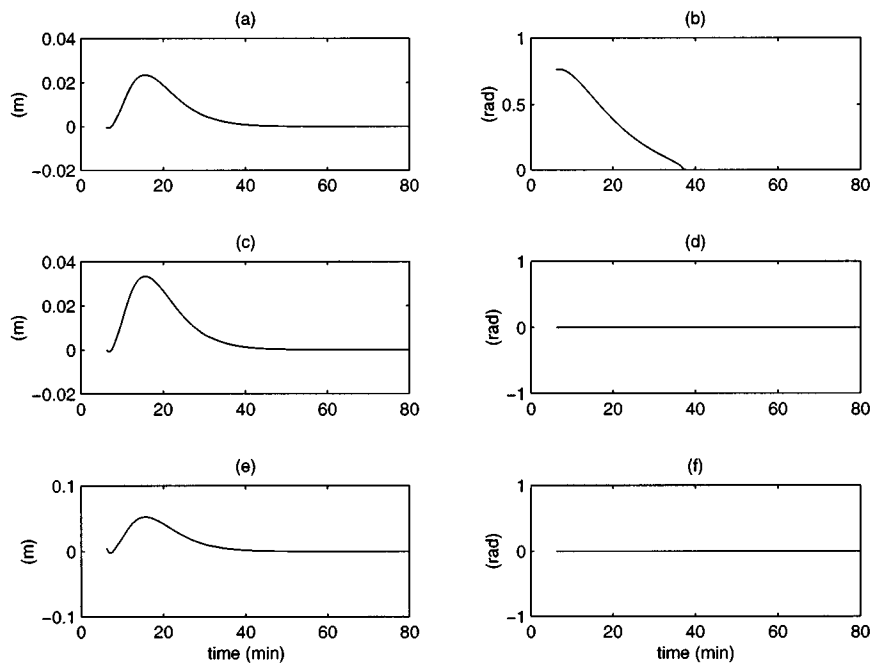


Fig. 7. Position and attitude errors in the transition from Mode 1 to Mode 2. (a) Absolute position error for Spacecraft #1. (b) Absolute attitude error for Spacecraft #1. (c) Relative position error between Spacecraft #1 and #2. (d) Relative attitude error between Spacecraft #1 and #2. (e) Relative position error between Spacecraft #1 and #3. (f) Relative attitude error between Spacecraft #1 and #3.

architecture to the problem of synthesizing a multiple spacecraft interferometer in deep space. The architecture introduced in the paper has several key features. First, the coordination mechanism is specifically identified as the states of the formation control block and the states of the supervisor. Second, feedback

to the formation is explicitly defined. Third, the architecture accommodates both centralized and decentralized implementations. Fourth, it is amenable to control theoretic techniques. Finally, it provides a uniform architecture to compare and contrast various approaches to formation control.

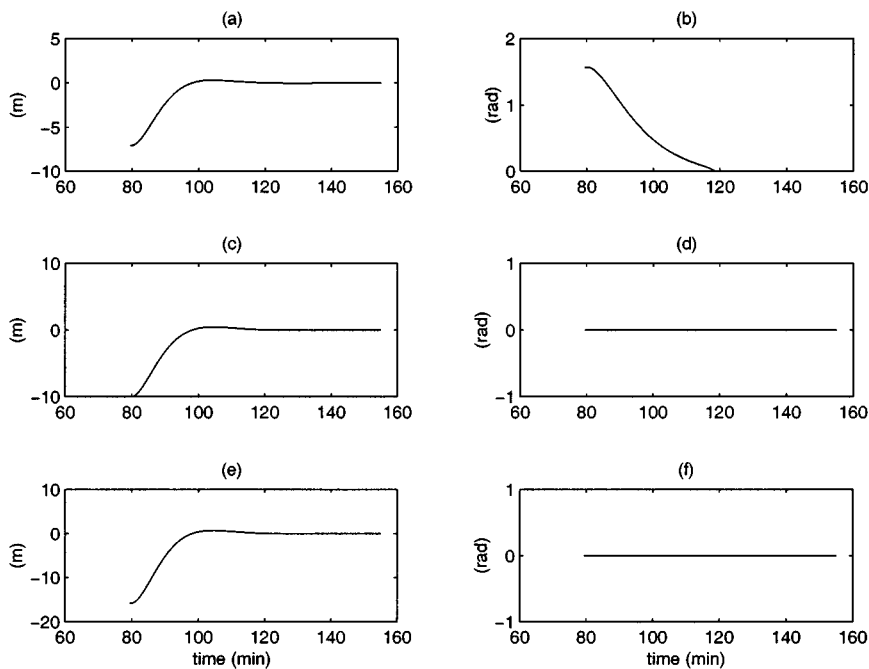


Fig. 8. Position and attitude errors in the transition from Mode 2 to Mode 3. (a) Absolute position error for Spacecraft #1. (b) Absolute attitude error for Spacecraft #1. (c) Relative position error between Spacecraft #1 and #2. (d) Relative attitude error between Spacecraft #1 and #2. (e) Relative position error between Spacecraft #1 and #3. (f) Relative attitude error between Spacecraft #1 and #3.

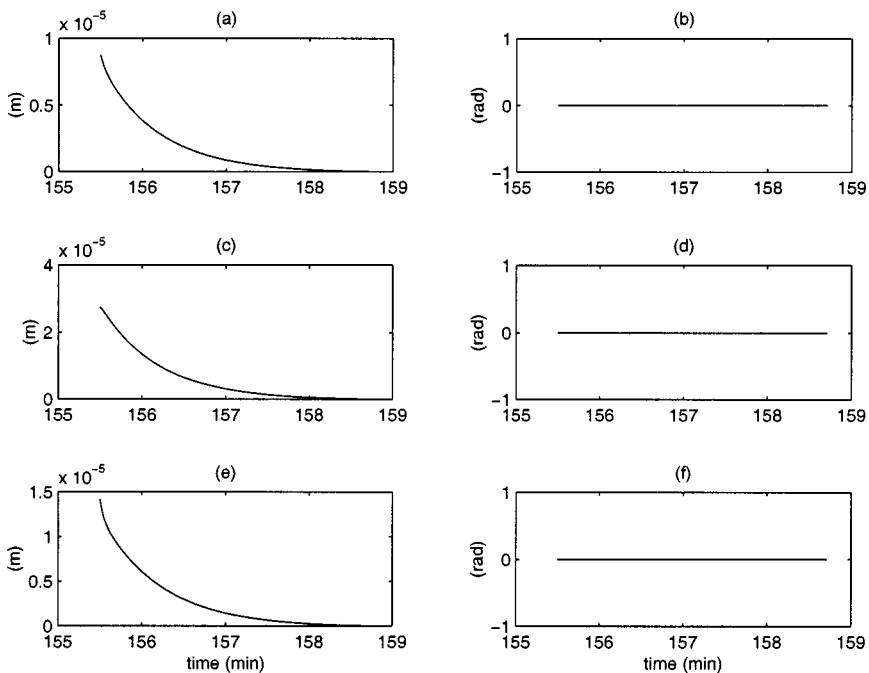


Fig. 9. Position and attitude errors in the transition from Mode 3 to Mode 4. (a) Absolute position error for Spacecraft #1. (b) Absolute attitude error for Spacecraft #1. (c) Relative position error between Spacecraft #1 and #2. (d) Relative attitude error between Spacecraft #1 and #2. (e) Relative position error between Spacecraft #1 and #3. (f) Relative attitude error between Spacecraft #1 and #3.

APPENDIX A
QUATERNION MANIPULATION

This Appendix contains a few facts about quaternions needed in the paper. For a more complete discussion of quaternions see [37] and [41]–[43].

Euler’s theorem for rigid body rotations states that “the general displacement of a rigid body with one point fixed is a rota-

tion about some axis” [44]. Let \mathbf{z} represent a unit vector in the direction of rotation, called the Euler axis or the eigenaxis, and let ϕ represent the angle of rotation about \mathbf{z} , called the Euler angle. The unit quaternion representing this rotation is given by

$$\mathbf{q} = \begin{pmatrix} \mathbf{z} \sin\left(\frac{\phi}{2}\right) \\ \cos\left(\frac{\phi}{2}\right) \end{pmatrix} \triangleq \begin{pmatrix} \vec{q} \\ \bar{q} \end{pmatrix}$$

where $\vec{\mathbf{q}} \in \mathbb{R}^3$ and \bar{q} is a scalar.

Given a vector $\mathbf{v} = (v_1 \ v_2 \ v_3)'$, let \mathbf{v}^\times denote the matrix

$$\mathbf{v}^\times = \begin{pmatrix} 0 & -v_3 & v_2 \\ v_3 & 0 & -v_1 \\ -v_2 & v_1 & 0 \end{pmatrix}.$$

Let \mathcal{C}_0 and \mathcal{C}_1 be two arbitrary coordinate frames. By Euler's theorem, the relative orientation of the two frames can be represented by a single rotation ϕ about an axis \mathbf{z} [44]. The direction cosine matrix representing this orientation is given by [37]

$$A(\mathbf{q}) = (2\bar{q}^2 - 1)\mathbf{I} + 2\tilde{\mathbf{q}}\tilde{\mathbf{q}}' + 2\bar{\mathbf{q}}\tilde{\mathbf{q}}^\times.$$

Vector rotations can also be represented by quaternion multiplications. Let \mathbf{q}^* be the inverse of a quaternion given by the formula

$$\mathbf{q}^* = \begin{pmatrix} \bar{\mathbf{q}} \\ \hat{q} \end{pmatrix}^* = \begin{pmatrix} -\bar{\mathbf{q}} \\ \hat{q} \end{pmatrix}.$$

Then the vector p_0 expressed in \mathcal{C}_0 , is expressed in \mathcal{C}_1 as

$$\begin{pmatrix} p_1 \\ 0 \end{pmatrix} = \mathbf{q}_0^1 \begin{pmatrix} p_0 \\ 0 \end{pmatrix} (\mathbf{q}_0^1)^*,$$

which will be written in the shorthand notation $p_1 = \mathbf{q}_0^1 p_0 (\mathbf{q}_0^1)^*$.

If $\mathbf{q} = (\bar{\mathbf{q}}', \bar{q})'$ represents the attitude of a rigid body, then the kinematic equations that relate the angular velocity of the rigid body to its attitude is given by the following equations [43]:

$$\begin{pmatrix} \dot{\bar{\mathbf{q}}} \\ \dot{\bar{q}} \end{pmatrix} = \begin{pmatrix} -\frac{1}{2}\boldsymbol{\omega} \times \bar{\mathbf{q}} + \frac{1}{2}\bar{q}\boldsymbol{\omega} \\ -\frac{1}{2}\boldsymbol{\omega} \cdot \bar{\mathbf{q}} \end{pmatrix} \triangleq \frac{1}{2}\Omega(\boldsymbol{\omega})\mathbf{q}.$$

Suppose that the unit quaternions \mathbf{q}_d and \mathbf{q} represent the desired attitude and the actual attitude of a rigid body, respectively, then the attitude error is given by $\mathbf{q}_e = \mathbf{q}^*\mathbf{q}_d$.

The set of unit quaternions represent a parameterization of $\text{SO}(3)$. A geodesic on $\text{SO}(3)$ is a differentiable parameterized path in $\text{SO}(3)$ connecting two rotations [42]. The distance between any two rotations is defined to be the shortest geodesic between those rotations. Let \mathbf{q}_1 and \mathbf{q}_2 be any two unit quaternions, in [42], it is shown that the shortest geodesic, called the "geodesic metric" $\rho(\mathbf{q}_1, \mathbf{q}_2)$ on $\text{SO}(3)$ between \mathbf{q}_1 and \mathbf{q}_2 is

$$\rho(\mathbf{q}_1, \mathbf{q}_2) = 2 \arccos(|\bar{q}_e|),$$

where

$$\mathbf{q}_e \triangleq \begin{pmatrix} \bar{\mathbf{q}}_e \\ \bar{q}_e \end{pmatrix} = \mathbf{q}_2^*\mathbf{q}_1.$$

APPENDIX B

PROOF OF LEMMA 1

Since the translational and rotational motion are decoupled, we can consider the convergence of

$$\begin{pmatrix} \|\mathbf{r} - \mathbf{r}^d\| \\ \|\mathbf{v} - \mathbf{v}^d\| \end{pmatrix} \quad \text{and} \quad \begin{pmatrix} \rho(\mathbf{q}, \mathbf{q}^d) \\ \|\boldsymbol{\omega} - \boldsymbol{\omega}^d\| \end{pmatrix}$$

separately.

The result for rotational motion is contained in [45, Theorem 1]. The proof for translation motion is inspired by the technique used in [45, Th. 1].

Let

$$\boldsymbol{\xi} \triangleq \begin{pmatrix} \mathbf{r} - \mathbf{r}^d \\ \dot{\mathbf{r}} - \dot{\mathbf{r}}^d \end{pmatrix}.$$

Then the dynamics in terms of $\boldsymbol{\xi}$ are

$$\dot{\boldsymbol{\xi}} = \begin{pmatrix} 0 & I \\ -K_r & -K_v \end{pmatrix} \boldsymbol{\xi} - \begin{pmatrix} 0 \\ I \end{pmatrix} \ddot{\mathbf{r}}^d \quad (9)$$

where K_r and K_v are positive definite matrices. Define the Lyapunov function candidate

$$V(\boldsymbol{\xi}) = \frac{1}{2}\boldsymbol{\xi}' \begin{pmatrix} K_r + cK_v & cI \\ cI & I \end{pmatrix} \boldsymbol{\xi}$$

which is positive definite for c sufficiently small since

$$\begin{pmatrix} K_r + cK_v & cI \\ cI & I \end{pmatrix} = \begin{pmatrix} I & cI \\ 0 & I \end{pmatrix} \begin{pmatrix} K_r + cK_v - c^2I & 0 \\ 0 & I \end{pmatrix} \begin{pmatrix} I & 0 \\ cI & I \end{pmatrix}.$$

Differentiating V we get

$$\dot{V} = \frac{1}{2}\boldsymbol{\xi}' \begin{pmatrix} K_r + cK_v & cI \\ cI & I \end{pmatrix} \dot{\boldsymbol{\xi}} + \frac{1}{2}\dot{\boldsymbol{\xi}}' \begin{pmatrix} K_r + cK_v & cI \\ cI & I \end{pmatrix} \boldsymbol{\xi}.$$

Substituting in from (9) and simplifying we get

$$\dot{V} = -\boldsymbol{\xi}' \begin{pmatrix} cK_r & 0 \\ 0 & K_v - cI \end{pmatrix} \boldsymbol{\xi} - \boldsymbol{\xi}' \begin{pmatrix} cI \\ I \end{pmatrix} \ddot{\mathbf{r}}^d.$$

Letting $L = \begin{pmatrix} cK_r & 0 \\ 0 & K_v - cI \end{pmatrix}$, and $Q = -\begin{pmatrix} cI \\ I \end{pmatrix}$ we get

$$\dot{V} = -\boldsymbol{\xi}' L \boldsymbol{\xi} + \boldsymbol{\xi}' Q \ddot{\mathbf{r}}^d$$

where L is positive definite for sufficiently small c .

Let $\underline{\sigma}(L)$ denote the minimum singular value of L , then

$$\dot{V} \leq -\underline{\sigma}(L)\|\boldsymbol{\xi}\|^2 + \boldsymbol{\xi}' Q \ddot{\mathbf{r}}^d.$$

Integrating this expression gives

$$\begin{aligned} V(\boldsymbol{\xi}(t)) - V(\boldsymbol{\xi}_0) &\leq \int_0^t (-\underline{\sigma}(L)\|\boldsymbol{\xi}(\tau)\|^2 + \boldsymbol{\xi}'(\tau)Q\ddot{\mathbf{r}}^d(\tau)) d\tau \\ &= -\underline{\sigma}(L) \int_0^t \|\boldsymbol{\xi}(\tau)\|^2 d\tau + \int_0^t \boldsymbol{\xi}'(\tau)Q\ddot{\mathbf{r}}^d(\tau) d\tau \\ &\leq -\underline{\sigma}(L) \int_0^t \|\boldsymbol{\xi}(\tau)\|^2 d\tau + \int_0^t \|\boldsymbol{\xi}(\tau)\| \|Q\ddot{\mathbf{r}}^d(\tau)\| d\tau \\ &\leq -\underline{\sigma}(L) \int_0^\infty \|\boldsymbol{\xi}(\tau)\|^2 d\tau + \int_0^\infty \|\boldsymbol{\xi}(\tau)\| \|Q\ddot{\mathbf{r}}^d(\tau)\| d\tau \\ &\leq -\underline{\sigma}(L)\|\boldsymbol{\xi}\|_{L_2}^2 + \|\boldsymbol{\xi}\|_{L_2} \|Q\ddot{\mathbf{r}}^d\|_{L_2} \end{aligned}$$

where $\|\boldsymbol{\xi}\|_{L_2}^2 = \int_0^\infty \|\boldsymbol{\xi}(\tau)\|^2 d\tau$, and where the second and fourth inequalities follow from the application of Schwartz inequality in \mathbb{R}^{2n} and L_2 , respectively. Since $V(\boldsymbol{\xi}(t)) > 0$ we have that

$$\|\boldsymbol{\xi}\|_{L_2}^2 - \frac{\|Q\ddot{\mathbf{r}}^d\|_{L_2}}{\underline{\sigma}(L)}\|\boldsymbol{\xi}\|_{L_2} - \frac{V(\boldsymbol{\xi}_0)}{\underline{\sigma}(L)} \leq 0.$$

Completing the squares gives

$$\left(\|\boldsymbol{\xi}\|_{L_2} - \frac{\|Q\ddot{\mathbf{r}}^d\|_{L_2}}{2\underline{\sigma}(L)} \right)^2 - \left(\frac{V(\boldsymbol{\xi}_0)}{\underline{\sigma}(L)} + \frac{\|Q\ddot{\mathbf{r}}^d\|_{L_2}^2}{4\underline{\sigma}(L)^2} \right) \leq 0.$$

Solving for $\|\xi\|_{L_2}$ gives

$$\|\xi\|_{L_2} \leq \frac{\|Q\ddot{r}^d\|_{L_2}}{2\sigma(L)} + \sqrt{\frac{\|Q\ddot{r}^d\|_{L_2}^2}{4\sigma(L)^2} + \frac{V(\xi_0)}{\sigma(L)}}.$$

Therefore $\ddot{r}^d \in L_2[0, \infty)$ implies that $\xi \in L_2[0, \infty)$. By hypothesis, (9) is a bounded input–bounded output stable linear system, therefore if $\ddot{r}^d \in L_\infty[0, \infty)$ then ξ remains bounded which implies that $\dot{\xi}$ is bounded. Therefore ξ is uniformly continuous and Barbalat’s lemma [46] implies that $\|\xi(t)\| \rightarrow 0$ as $t \rightarrow \infty$.

REFERENCES

- [1] P. K. C. Wang, “Navigation strategies for multiple autonomous mobile robots moving in formation,” *J. Robot. Syst.*, vol. 8, no. 2, pp. 177–195, 1991.
- [2] P. K. C. Wang and F. Y. Hadaegh, “Coordination and control of multiple microspacecraft moving in formation,” *J. Astronautical Sci.*, vol. 44, no. 3, pp. 315–355, 1996.
- [3] P. K. C. Wang, F. Hadaegh, and K. Lau, “Synchronized formation rotation and attitude control of multiple free-flying spacecraft,” *AIAA J. Guidance, Contr. Dynamics*, vol. 22, pp. 28–35, Jan. 1999.
- [4] F. Y. Hadaegh, W.-M. Lu, and P. K. C. Wang, “Adaptive control of formation flying spacecraft for interferometry,” in *Proc. Int. Federation Automat. Contr.*, 1998.
- [5] Q. Yan, G. Yang, V. Kapila, and M. S. de Queiroz, “Nonlinear dynamics and adaptive control of multiple spacecraft in periodic relative orbits,” in *23rd Annu. AAS Guidance Contr. Conf.*. Breckenridge, CO: Amer. Astronautical Soc., Feb. 2000, pp. AAS 00–013.
- [6] V. Kapila, A. G. Sparks, J. M. Buffington, and Q. Yan, “Spacecraft formation flying: Dynamics and control,” *J. Guidance, Contr. Dyn.*, vol. 23, pp. 561–564, May–June 2000.
- [7] M. S. de Queiroz, V. Kapila, and Q. Yan, “Adaptive nonlinear control of multiple spacecraft formation flying,” *J. Guidance, Contr. Dyn.*, vol. 23, pp. 385–390, May–June 2000.
- [8] T. Sugar and V. Kumar, “Decentralized control of cooperating mobile manipulators,” in *Proc. IEEE Int. Conf. Robot. Automat.*, Leuven, Belgium, May 1998, pp. 2916–2921.
- [9] J. P. Desai, J. Ostrowski, and V. Kumar, “Controlling formations of multiple mobile robots,” in *Proc. IEEE Int. Conf. Robot. Automat.*, Leuven, Belgium, May 1998, pp. 2864–2869.
- [10] H. Yamaguchi and J. W. Burdick, “Asymptotic stabilization of multiple nonholonomic mobile robots forming group formations,” in *Proc. IEEE Int. Conf. Robot. Automat.*, Leuven, Belgium, May 1998, pp. 3573–3580.
- [11] S. Sheikholeslam and C. A. Desoer, “Control of interconnected nonlinear dynamical systems: The platoon problem,” *IEEE Trans. Automat. Contr.*, vol. 37, pp. 806–810, June 1992.
- [12] C. R. McInnes, “Autonomous ring formation for a planar constellation of satellites,” *J. Guidance, Contr. Dyn.*, vol. 18, no. 5, pp. 1215–1217, 1995.
- [13] M. R. Anderson and A. C. Robbins, “Formation flight as a cooperative game,” in *Proc. AIAA Guidance, Navigation, Contr. Conf.*. Boston, MA: Amer. Inst. Aeronautics Astronautics, AIAA-98–4124, Aug. 1998, pp. 244–251.
- [14] T. Balch and R. C. Arkin, “Behavior-based formation control for multi-robot teams,” *IEEE Trans. Robot. Automat.*, vol. 14, pp. 926–939, Dec. 1998.
- [15] X. Yun, G. Alptekin, and O. Albayrak, “Line and circle formation of distributed physical mobile robots,” *J. Robot. Syst.*, vol. 14, no. 2, pp. 63–76, 1997.
- [16] Q. Chen and J. Y. S. Luh, “Coordination and control of a group of small mobile robots,” in *Proc. IEEE Int. Conf. Robot. Automat.*, 1994, pp. 2315–2320.
- [17] M. A. Lewis and K.-H. Tan, “High precision formation control of mobile robots using virtual structures,” *Autonomous Robot.*, vol. 4, pp. 387–403, 1997.
- [18] R. W. Beard and F. Y. Hadaegh, “Constellation templates: An approach to autonomous formation flying,” in *Proc. World Automat. Congress*. Anchorage, AK: ISIAAC, May 1998, pp. 177.1–177.6.
- [19] R. W. Beard, “Architecture and algorithms for constellation control,” Jet Propulsion Lab., California Inst. Technol., Pasadena, CA, Tech. Rep., Mar. 1998.
- [20] C. Scolese, D. Folta, and F. Bordini, “Field of view location and formation flying for polar orbiting missions,” in *Proc. AAS/AIAA Spaceflight Mechanics Meet.: Advances Astronautical Sci.*, vol. 75, 1991, pp. 949–966.
- [21] D. Folta, F. Bordini, and C. Scolese, “Considerations on formation flying separations for earth observing satellite missions,” *Proc. AAS/AIAA Spaceflight Mechanics Meet.: Advances Astronautical Sci.*, vol. 79, no. 2, pp. 803–822, 1992.
- [22] D. Folta and D. Quinn, “A universal 3-D method for controlling the relative motion of multiple spacecraft in any orbit,” in *AIAA Guidance, Navigation, Contr. Conf.*, Boston, MA, Aug. 1998.
- [23] M. A. Vincent, “Design of the TOPSAT mission,” *Proc. AAS/AIAA Astrodynamics Meet.*, vol. 85, no. 2, pp. 1137–1146, 1993.
- [24] R. E. Glickman, “TIDE: The timed-destination approach to constellation formation keeping,” *Proc. AAS/AIAA Spaceflight Mechanics Meet.: Advances Astronautical Sci.*, vol. 87, no. 2, pp. 725–743, 1994.
- [25] Y. Ulybyshev, “Long-term formation keeping of satellite constellation using linear-quadratic controller,” *J. Guidance, Contr. Dyn.*, vol. 21, pp. 109–115, Jan.–Feb. 1998.
- [26] P. K. C. Wang and F. Y. Hadaegh, “Minimum-fuel formation reconfiguration of multiple free-flying spacecraft,” Univ. California, Los Angeles, ENG 97-187, Dec. 1997.
- [27] R. W. Beard and F. Y. Hadaegh, “Fuel optimization for unconstrained rotation of spacecraft formations,” *J. Astronautical Sci.*, vol. 43, pp. 259–273, July–Dec. 1999.
- [28] R. W. Beard, T. W. McLain, and F. Y. Hadaegh, “Fuel optimization for constrained rotation of spacecraft formations,” *AIAA J. Guidance, Contr. Dyn.*, vol. 23, pp. 339–346, Mar.–Apr. 2000.
- [29] W. Kang, N. Xi, and A. Sparks, “Formation control of autonomous agents in 3-D workspace,” in *Proc. IEEE Int. Conf. Robot. Automat.*, San Francisco, CA, Apr. 2000, pp. 1755–1760.
- [30] P. Varaiya, “Smart cars on smart roads: Problems of control,” *IEEE Trans. Automat. Contr.*, vol. 38, pp. 195–207, Feb. 1993.
- [31] S. Sastry, G. Meyer, C. Tomlin, J. Lygeros, D. Godbole, and G. Pappas, “Hybrid control in air traffic management systems,” in *Proc. 34th IEEE Conf. Decision Contr.*, New Orleans, LA, 1995, pp. 1478–1483.
- [32] C. P. Sanders, P. A. DeBitetto, E. Feron, H. F. Vuong, and N. Leveson, “Hierarchical control of small autonomous helicopters,” in *Proc. 37th IEEE Conf. Decision. Contr.*, Tampa, FL, Dec. 1998, pp. 3629–3634.
- [33] T. M. Cover and J. A. Thomas, *Elements of Information Theory*. New York: Wiley, 1991.
- [34] K. Lau, M. Colavita, and M. Shao. The new millennium separated spacecraft interferometer. [Online]. Available: <http://www.spacebase.jpl.nasa.gov>
- [35] K. Lau, S. Lichten, L. Young, and B. Haines, “An innovative deep space application of GPS technology for formation flying spacecraft,” in *Amer. Inst. Aeronautics, Astronautics, Guidance, Navigation, Contr. Conf.*, July 1996, pp. 96–381.
- [36] S. S. Joshi, “An informal introduction to synthetic aperture imaging,” Jet Propulsion Lab, Pasadena, CA, Interoffice Memo. 3450-98-0004, Feb. 1998.
- [37] J. R. Wertz, Ed., *Spacecraft Attitude Determination and Control*. Boston, MA: Kluwer, 1978.
- [38] D. T. Greenwood, *Principles of Dynamics*, 2nd ed. Englewood Cliffs, NJ: Prentice-Hall, 1988.
- [39] R. W. Beard, T. W. McLain, and F. Y. Hadaegh, “Fuel equalized retargeting for separated spacecraft interferometry,” in *Proc. Amer. Contr. Conf.*, Philadelphia, PA, June 1998, pp. 1580–1584.
- [40] R. W. Beard and F. Y. Hadaegh, “Fuel optimized rotation for satellite formations in free space,” in *Proc. Amer. Contr. Conf.*, San Diego, CA, June 1999, pp. 2975–2979.
- [41] M. D. Shuster, “A survey of attitude representations,” *J. Astronautical Sci.*, vol. 41, pp. 439–517, Oct. 1993.
- [42] C. Samsom, M. Le Borgne, and B. Espiau, *Robot Control: A Task Function Approach*. Oxford, U.K.: Oxford Science, 1991.
- [43] M. J. Sidi, *Spacecraft Dynamics and Control*, ser. Cambridge Aerospace: Cambridge Univ. Press, 1997.
- [44] H. Goldstein, *Classical Mechanics*. Reading, MA: Addison-Wesley, 1951.
- [45] J. T.-Y. Wen and K. Kreutz-Delgado, “The attitude control problem,” *IEEE Trans. Automat. Contr.*, vol. 36, pp. 1148–1162, Oct. 1991.
- [46] H. K. Khalil, *Nonlinear Systems*, 2nd ed. Upper Saddle River, NJ: Prentice-Hall, 1996.



Randal W. Beard (S'91–M'92) received the B.S. degree in electrical engineering from the University of Utah, Salt Lake City, in 1991, the M.S. degree in electrical engineering in 1993, the M.S. degree in mathematics in 1994, and the Ph.D. degree in electrical engineering in 1995, all from Rensselaer Polytechnic Institute, Troy, NY.

Since 1996, he has been an Assistant Professor in the Electrical and Computer Engineering Department at Brigham Young University, Provo, UT. In 1997 and 1998, he was a Summer Faculty Fellow at the Jet Propulsion Laboratory, California Institute of Technology, Pasadena, CA. His research interests include coordinated control of multiple vehicle systems and nonlinear and optimal control.

Dr. Beard is a member of AIAA and Tau Beta Pi and is currently an Associate Editor for the IEEE Control Systems Society Conference Editorial Board.



Jonathan Lawton (S'98–M'00) received the B.S. degree in physics in 1994, the M.S. degree in mathematics in 1997, and the Ph.D. degree in electrical engineering in 2000, all from Brigham Young University, Provo, UT.

He is currently on the technical staff at Raytheon Systems Company, Tucson, AZ. His research interests include Kalman filtering, attitude control, and coordinated spacecraft formation flying.



Fred Y. Hadaegh (S'75–M'80–SM'89) received the B.S.E.E. degree with honors and the M.S.E.E. degree, both from the University of Texas, Austin, and the Ph.D. degree in electrical engineering from the University of Southern California, Los Angeles.

He joined the Jet Propulsion Laboratory (JPL), California Institute of Technology, Pasadena, in 1984. He is currently a Senior Research Scientist and Technical Supervisor for the Guidance and Control Analysis Group. In addition, he is the Manager of the Distributed Spacecraft Technology Program at

JPL. His research interests are in the areas of system identification, estimation theory, and spacecraft control analysis and design. He has published extensively on mathematical modeling of uncertain systems, parameter identifiability, identification and control of large-space structures, and autonomous control of formation flying space systems.

Dr. Hadaegh is an Association Fellow of AIAA, a former Associate Editor of the IEEE TRANSACTIONS ON CONTROL SYSTEMS TECHNOLOGY, and member of Eta Kappa Nu and Sigma Xi. He has received NASA's Exceptional Service Medal and NASA's Exceptional Achievement Medal. He has also received numerous NASA New Technology Awards. He serves in various professional organizations and on technical committees.